Weak localization in $Al_xGa_{1-x}As/GaAs/Al_xGa_{1-x}As$ heterostructures with electrostatically induced random antidot array

G. M. Minkov and A. A. Sherstobitov
Institute of Metal Physics, RAS, 620041 Ekaterinburg, Russia

A. V. Germanenko and O. E. Rut
Institute of Physics and Applied Mathematics, Ural State University, 620083 Ekaterinburg, Russia

(Received 7 June 2008; revised manuscript received 24 October 2008; published 19 November 2008)

Results of experimental study of the weak localization in gated $Al_xGa_{1-x}As/GaAs/Al_xGa_{1-x}As$ structures with artificial inhomogeneity of potential relief are presented. It has been found that the shape of the magnetoconductivity curve differs significantly from that measured for the homogeneous two-dimensional gas. This difference is shown to be caused by the difference in statistics of closed paths. The area distribution function of closed paths has been obtained using the Fourier transformation of the experimental magnetoconductivity curves taken at different temperatures. The results obtained are in qualitative agreement with the results of computer simulation.

DOI: 10.1103/PhysRevB.78.195319 PACS number(s): 73.20.Fz, 73.61.Ey

The transport properties of two-dimensional (2D) semiconductor structures with antidots array were intensively studied both experimentally[1–11] and theoretically[12–16] in the last 10–15 years. The main concern was with the investigations of the ballistic systems, in which $l > d, D$, where l is the mean free path, d and D are the size of antidots and the period of antidots array, respectively. The rich diversity of the transport phenomena, such as commensurable oscillations, the peculiarities due to the trajectories rolling along the array of antidots, was observed. The antidots array structures in the diffusion regime ($l < d, D$) were not studied essentially. Such structures are interesting in some aspects. First of all, the quantum corrections to the conductivity due to weak localization (WL) and electron-electron (e-e) interaction have to reveal the specific features when the phase breaking length $L_\phi = \sqrt{\mathcal{D}\tau_\phi}$ (where $\mathcal{D}$ is the diffusion coefficient, τ_ϕ is phase breaking time) or the temperature length $L_T = \sqrt{\mathcal{D}/T}$ (hereafter, we set $k_B = 1$ and $\hbar = 1$) becomes larger than d, D with the temperature decrease. Second, the large enough negative gate voltage has to deplete the channels between the antidots (the channel width w_0 is about $D - d$) and as a result has to lead to crossover to the hopping conductivity. Besides, from the transport properties standpoint, the antidots arrays are the fine model of the granular media. In contrast to the granular metallic film, the parameters of the "granules" and "barriers" are reliably known and can be changed continuously within wide range.

In this paper, we report the results of experimental study of the weak localization correction to the conductivity in the structure with the random array of antidots. An analysis of the experimental results and its comparison with the results of computer simulation show that the changes in the magnetoconductivity curves which are observed, when the dielectric inclusions in 2D gas under the antidots are formed and grow in size, result from a change in the statistics of the closed paths. Namely, the contribution of the trajectories with the large enclosed area is strongly suppressed.

The random antidots array was made on the single-quantum well heterostructure with the electron density $n = 1.5 \times 10^{12}$ cm^{-2} and mobility $\mu = 19\,000$ cm^2/(V s) grown by the molecular-beam epitaxy. It consists of a 250-nm-thick-undoped GaAs buffer layer grown on semi-insulator GaAs, a 50-nm-$Al_{0.3}Ga_{0.7}As$ barrier, Si δ layer, a 6 nm spacer of undoped $Al_{0.3}Ga_{0.7}As$, an 8 nm GaAs well, a 6 nm spacer of undoped $Al_{0.3}Ga_{0.7}As$, a Si δ layer, a 50 nm $Al_{0.3}Ga_{0.7}As$ barrier, and 150-nm-cap layer of undoped GaAs [Fig. 1(a)]. The samples were etched into standard Hall bars. The holes in the cap layer [Fig. 1(b)] were fabricated with the use of electron-beam lithography and wet etching. Their depth measured by atomic force microscope (AFM) consists of about 85 nm. Note that this depth is less than the cap layer thickness before etching. The holes of 0.7 μm diameter were shifted randomly on the value ≈ 0.1 μm from the sites of the square lattice with the period of about 1 μm. This shift destroys all oscillations in the galvanomagnetic effects resulted from the commensurability between the cyclotron orbits and the lattice period and from the trajectories rolling along the array of antidots. After etching, an Al gate electrode was deposited by thermal evaporation onto the cap layer. Varying the gate voltage V_g from 1 to −3.7 V, we decreased the electron density in the quantum well from 1.8×10^{12} to 3×10^{11} cm^{-2}. Analysis of the Shubnikov de Haas (SdH) oscillations performed for different gate voltages shows that only one subband is occupied at $V_g < 0$. At positive gate voltage, the oscillations have two frequencies: one

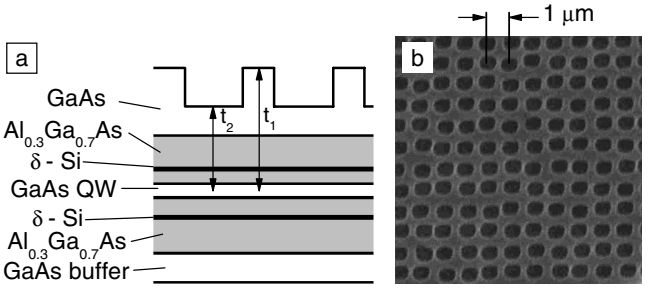

FIG. 1. (a) The sketch and (b) electron microscope image of the structure investigated.

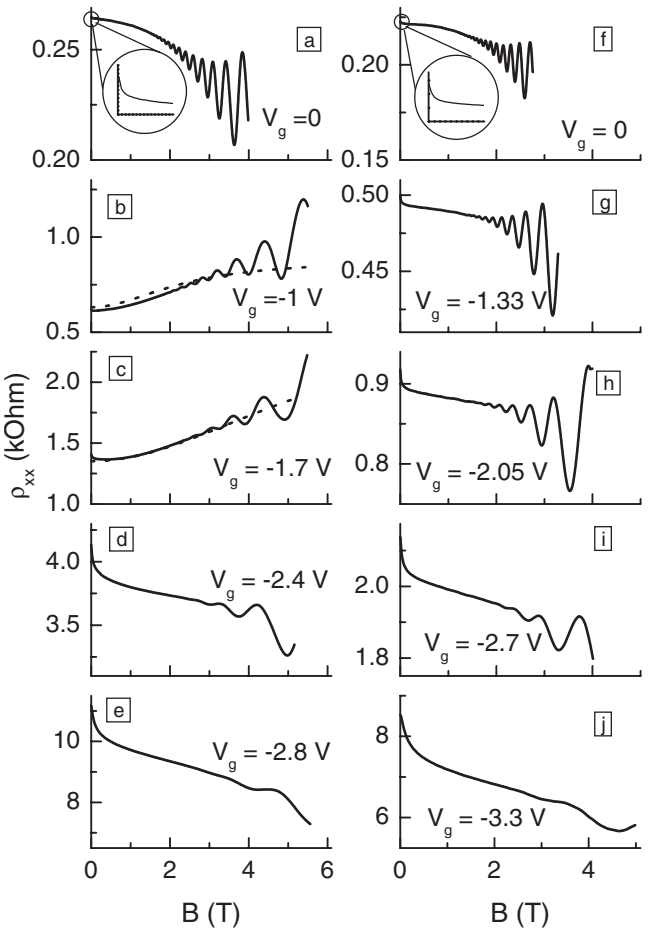

FIG. 2. The magnetic-field dependences of ρ_{xx} for the patterned (left column) and unpatterned (right column) structures for $T=4.2$ K. The dotted lines in (b) and (c) are calculated from the standard classical formula for two types of carriers with the electron densities found from Eqs. (1) and (2) and $\mu_1=12600$ cm^2/(V s), $\mu_2=3400$ cm^2/(V s) for $V_g=-1$ V, and $\mu_1=8600$ cm^2/(V s), $\mu_2=1300$ cm^2/(V s) for $V_g=-2.4$ V that corresponds to the model described in the text.

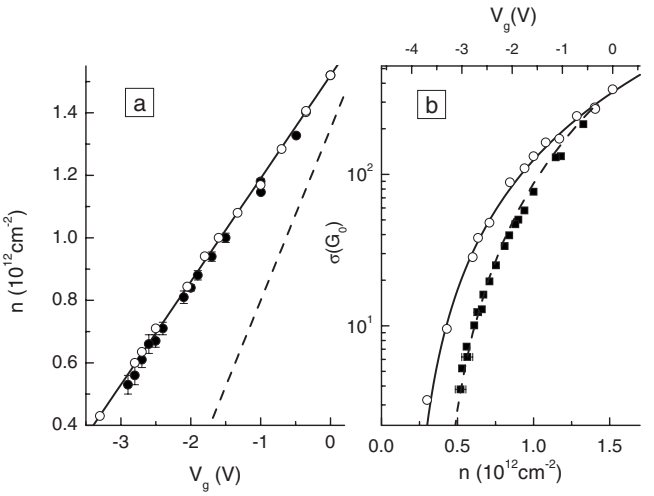

FIG. 3. (a) The gate voltage dependence of the electron density found from the SdH oscillations for the patterned (solid symbols) and unpatterned (open symbols) structures. Solid and dashed lines are drawn according to Eqs. (1) and (2), respectively. (b) The electron-density dependences of the conductivity measured at $T=4.2$ K for the patterned (solid symbols) and unpatterned (open symbols) samples.

of them tends to zero at V_g about 0.2 V. This conclusion accords well with the results of the voltage-capacitance measurements and with the results of measurements of the Hall effect carried out at different V_g. In what follows we analyze the results obtained for $V_g \leq 0$ V, when the excited subbands lay far above the Fermi level and are practically empty for the actual temperature range.

The magnetic-field dependences of the longitudinal resistance (ρ_{xx}) for the patterned structure together with that for the unpatterned one for some gate voltages are shown in Fig. 2. It is seen that they are rather complicated. Following the sharp magnetoresistivity in low magnetic field, which results from the suppression of the interference quantum correction, the relatively smooth negative or positive magnetoresistivity against the background of the SdH oscillations is observed.

Let us first consider the range of high magnetic field. At $V_g=0$ the magnetoresistances in the patterned and unpatterned structures are very close to each other [Figs. 2(a) and 2(f)]. In both cases, the paraboliclike negative magnetoresistance resulting from the *e-e* interaction correction (for more detail see Ref. 17) and the SdH oscillations of close frequency are observed. Such a behavior is not surprising, since the difference in local electron densities in the quantum well under the holes and outside them δn is relatively small at $V_g=0$. It can be estimated as $\delta n \approx (C_2-C_1)V_s/|e|$, where V_s is the surface potential, $C_{1,2}=\varepsilon\varepsilon_0/t_{1,2}$ is the local capacity, $t_{1,2}$ is the distance between 2D gas and gate electrode in different locations of the structure [see Fig. 1(a)], and ε_0 is dielectric constant of free space. With the use of $V_s=0.7$ V, $t_1=210$ nm, $t_2=125$ nm, and $\varepsilon=12.5$, we obtain $\delta n/n \approx 0.1$. However, δn strongly increases with the lowering gate voltage that leads to the positive magnetoresistance evident in the patterned sample within the gate voltage range from -1 to -1.8 V. The rise of the positive magnetoresistance is a sequence of the comparable contributions to the conductivity from the regions under the holes and out of them. For the first approximation, the transport in such inhomogeneous media can be considered as determined by two types of carriers with the different mobility and density.[18] The dotted curves in Figs. 2(b) and 2(c) are the magnetoresistivity calculated in the framework of this simple model with parameters determined below. At $V_g<-1.8$ V, the negative magnetoresistance is restored because the dielectric holes in 2D gas are formed and the conductivity of the structure is determined by the channels between the antidots.

The SdH oscillations in the patterned structure are observed down to $V_g \simeq -3$ V (Fig. 2). The periods of the oscillations in the patterned and unpatterned structures at given V_g are close to each other [see Fig. 3(a)], and the gate voltage dependence of the electron density calculated from the oscillations is well described by the expression

$$n_1(V_g) = n(V_g) = (1.52 + 0.33V_g) \times 10^{12} \text{ cm}^{-2}. \quad (1)$$

The fact that the oscillations of only one period are observed in the patterned sample and the dependences $n_1(V_g)$ and

$n(V_g)$ are practically the same mean that only the areas of 2D gas located out of the holes contribute to the SdH oscillations. One of the possible reasons is that the areas under various holes have different electron density due to the different depths of the holes. The potential relief due to nonflatness of the hole bottom is quite a plausible reason as well. The V_g dependence of the electron density under the holes $n_2(V_g)$ can be obtained from the geometric consideration. With the use of the local cap layer thickness $t_2=125$ nm, we have

$$n_2(V_g) = (1.35 + 0.55V_g) \times 10^{12} \text{ cm}^{-2}. \quad (2)$$

In Fig. 3(a) this dependence is shown by a dashed line.

Thus analyzing the high-field magnetoresistivity, we reason that (i) at $V_g < -1.8$ V the conductivity is mainly determined by the channels and (ii) the electron density out of the dielectric holes remains more or less homogeneous at these gate voltages.

Let us compare the behavior of the conductivity for the patterned (σ_{patt}) and unpatterned (σ_{unpatt}) samples at $B=0$. The values of σ_{patt} and σ_{unpatt} measured at $T=4.2$ K are plotted against the electron density found from the SdH oscillations in Fig. 3(b). It is seen that the conductivity of the patterned structure falls down significantly steeper with decreasing n than in the case of the unpatterned sample. Qualitatively such a behavior is transparent. This is because the 2D gas under the holes in the patterned sample is depleted faster with lowering V_g than that out of them due to thinner cap layer in these locations. If this is the case, we can obtain the geometrical parameters of the conducting areas knowing the experimental value of the ratio $\sigma_{\text{unpatt}}/\sigma_{\text{patt}}$ referred below as K. Using the data obtained for the unpatterned structure we obtain the mean free path, $l \simeq 0.03, \ldots, 0.3$ μm depending on the gate voltage, being less than the characteristic scales of the holes and channels ~ 0.5 μm [see Fig. 1(b)]. Therefore, one can deal with the local conductivity. If one additionally neglects the randomness in the antidots position, we can write out the following approximate expression for the conductivity of the patterned structure:

$$\sigma_{\text{patt}} \simeq \left\{ \int_0^D \frac{dy}{\sigma_1 w(y) + \sigma_2 [D - w(y)]} \right\}^{-1}, \quad (3)$$

where σ_1 and σ_2 stand for the local conductivity of the 2D gas out of and under the holes [in the inset in Fig. 4(a), these areas are labeled as 1 and 2, respectively], $w(y)$ is the y dependent width of the area 1. In what follows we suppose the area 2 is round in shape. The above equation gives the result, which coincides with the exact solution with the accuracy better than 20% when $w_0/D > 0.1$, where $w_0 = w(D/2)$ [see the inset in Fig. 4(a)]. In order to calculate the dependence $K(V_g)$, we assume that the local conductivity σ_1 and σ_2 is fully determined by the local electron density n_1 and n_2, respectively, and the σ_i-vs-n_i behavior is just the same as that for the unpatterned sample: $\sigma_1(n_1) = \sigma_{\text{unpatt}}(n)$ and $\sigma_2(n_2) = \sigma_{\text{unpatt}}(n)$ [shown by open symbols in Fig. 3(b)]. This assumption is natural because the main scattering mechanism in such low-mobility structures is the roughness of the interfaces forming the quantum well.

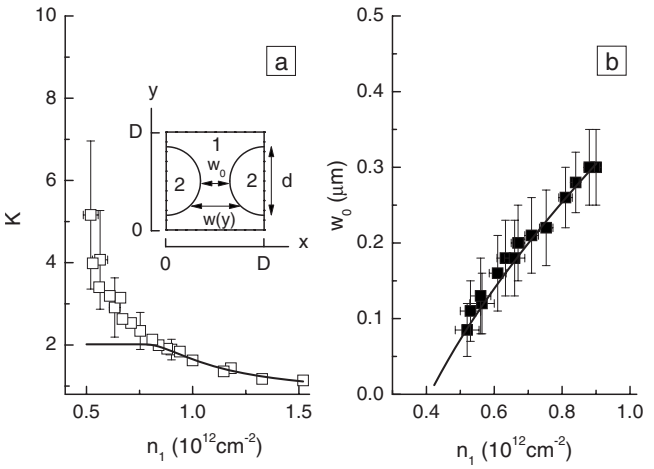

FIG. 4. (a) The K vs n_1 dependence obtained experimentally (symbols) and calculated from Eq. (3) (lines) for $d=0.7$ μm and $D=1$ μm. The inset shows one period of the antidots array. (b) The n_1 dependence of the channel width w_0 obtained from the experimental values of K at low V_g with the help of Eq. (3). The line is provided as a guide for the eyes.

In Fig. 4(a) we present the K-vs-n_1 dependences as they have been obtained experimentally and calculated from Eq. (3) with $d=0.7$ μm obtained from AFM. It is seen that this equation describes the experimental results only at $n_1 \gtrsim 8.5 \times 10^{11}$ cm^{-2} (that corresponds to $V_g \gtrsim -2$ V). At lower electron density the calculated curve demonstrates saturation, whereas the experimental plot continues to grow with lowering n. The reason for the discrepancy is transparent. When calculating the curve we kept d fixed. In this case K saturates with lowering n_1 as soon as σ_2 becomes much less than σ_1. The enhancement of K obtained experimentally for these gate voltages is a consequence of the depletion of the area outside the antidots, i.e., of an increase of the antidots size d and decrease of the channel width $w_0 = D - d$. Thus knowing the experimental value of K and using Eq. (3) we are able to find the channel width w_0 when $n_1 \lesssim 8.5 \times 10^{11}$ cm^{-2}. The results are depicted in Fig. 4(b). It is seen that w_0 really decreases when n_1 decreases. Extrapolating the w_0 vs n_1 plot to $w_0=0$, one obtains that the antidots close when $n_1 \simeq 4 \times 10^{11}$ cm^{-2} [$V_g = -(3.4, \ldots, 3.2)$ V].

Thus, the gate voltage dependence of the conductivity and the high magnetic-field magnetoresistance are reasonably described within the following simple model. At $V_g \gtrsim -2$ V the conductivity is determined both by the areas under the holes and out of them. These areas are characterized by the different electron density, which determines the local conductivity. At $V_g \simeq -(2, \ldots, 3)$ V the antidots are formed and the conductivity of structure is determined by the channels between the antidots with the local conductivity σ_1 equal to the conductivity σ of the unpatterned sample at the same electron density. Finally, at $V_g = -(3.4, \ldots, 3.2)$ V the channels are collapsed and most likely the crossover to the hopping conductivity occurs.

Let us now inspect the low magnetic-field negative magnetoresistivity which results from the suppression of the WL

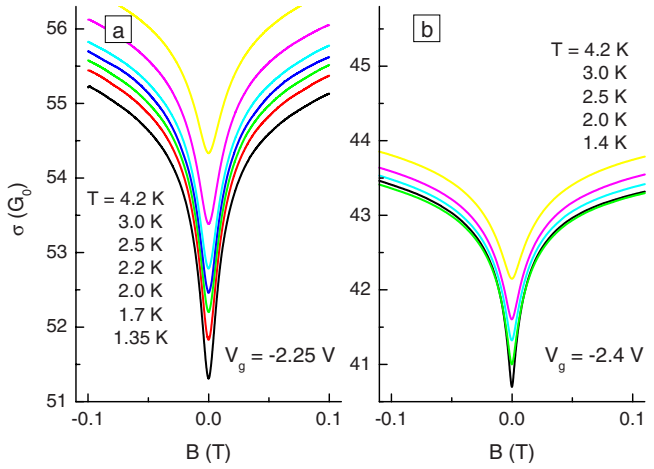

FIG. 5. (Color online) The low-field magnetoconductivity for different temperatures for the patterned (a) and unpatterned (b) structures. The local conductivity is shown in panel (a).

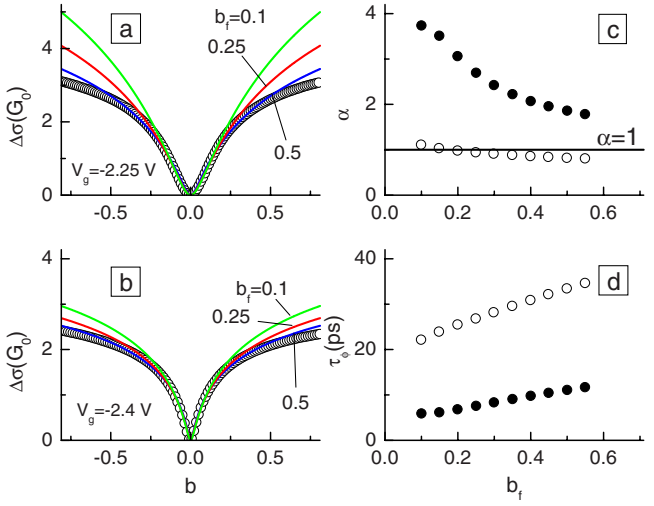

FIG. 6. (Color online) (a) and (b) The magnetoconductivity $\Delta\sigma$ as a function of normalized magnetic field $b=B/B_{\rm tr}$ for the lowest temperatures for the patterned (a) and unpatterned (b) samples. Symbols are the experimental results. Lines are the results of the best fit by Eq. (4) carried out within the different magnetic-field range $b=-b_f,\ldots,b_f$. (c) and (d) The fitting parameters α and τ_ϕ, respectively, for the patterned (solid symbols) and unpatterned (open symbols) samples as a function of the width of the fitting interval. The value of $B_{\rm tr}$ is $\simeq 0.05$ T for the patterned sample and $\simeq 0.07$ T for the unpatterned one.

correction. We focus our consideration on the results obtained within the second range of the gate voltages: $V_g \simeq -(2,\ldots,3)$ V. The magnetic-field dependences of the local conductivity measured in units of $G_0=e^2/(2\pi^2\hbar) \simeq 1.23\times 10^{-3}\ \Omega^{-1}$ are presented for different temperatures in Fig. 5(a). For comparison, the analogous dependences for the unpatterned structure measured at close conductivity values are shown in Fig. 5(b). It is seen that they are different; the conductivity change in the patterned sample is larger than that in the unpatterned one. As will be shown below, this difference results from the fact that the confinement of the electron paths increases the number of closed loops.

The difference in magnetoresistivity shape becomes all the more evident when comparing the results of data treatment performed in a standard manner. The shape of low-field positive magnetoconductivity $\Delta\sigma(B)=\rho_{xx}^{-1}(B)-\rho_{xx}^{-1}(0)$ caused by suppression of the weak localization in homogeneous 2D gas is described by the Hikami-Larkin-Nagaoka (HLN) expression,[19,20]

$$\Delta\sigma(b) = \alpha G_0\left[\psi\left(\frac{1}{2}+\frac{1}{b}\frac{\tau}{\tau_\phi}\right)-\psi\left(\frac{1}{2}+\frac{1}{b}\right)-\ln\frac{\tau}{\tau_\phi}\right], \quad (4)$$

where $b=B/B_{\rm tr}$, $B_{\rm tr}=\hbar/(2el^2)$ is the transport magnetic field, τ is the transport relaxation time, $\psi(x)$ is a digamma function, and α is the prefactor, which is equal to unity in the diffusion regime $(b<1, \tau \ll \tau_\phi)$ at high conductivity $(\sigma \gg G_0)$.

We have used this expression to fit each experimental curve with α and τ_ϕ as the fitting parameters within the different ranges of magnetic field $b=-b_f,\ldots,b_f$. Shown in Figs. 6(a) and 6(b) are the results of the fitting procedure carried out for the patterned and unpatterned samples, respectively, for the lowest temperature. The dependences of the fitting parameters τ_ϕ and α on the width of the fitting interval are shown in Figs. 6(c) and 6(d), respectively. One can see that the parameters found for the unpatterned structure behave themselves reasonably. The prefactor α is close to the unity independently of that in which interval the fit is made. Some rise of τ_ϕ with the extending fitting interval evident in Fig. 6(d) is a sequence of the fact that the magnetic-field dependence of τ_ϕ is not taken into account in Eq. (4).[21] At once, the temperature dependence of τ_ϕ is close to the theoretical one $\tau_\phi \propto 1/T$ [Fig. 7(a)], and the prefactor does not depend on the temperature [Fig. 7(b)]. Thus, the HLN expression well describes $\Delta\sigma(B)$ for the unpatterned sample.

In contrast to this, the strong sensitivity of the fitting parameters to the fitting interval takes place for the patterned sample. Therewith the value of α is significantly larger than

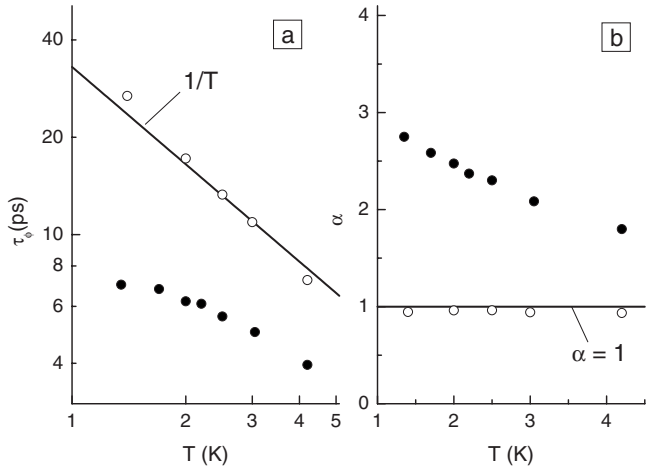

FIG. 7. The temperature dependence of the parameters (a) τ_ϕ and (b) α found from the fit of the experimental $\Delta\sigma$ vs B curves for the patterned (solid symbols) and unpatterned (open symbols) samples within the fitting interval of b from −0.25 to 0.25.

unity and strongly dependent on the temperature [Fig. 7(b)]. The value of the fitting parameter τ_ϕ is much less than that for the unpatterned structure and it saturates with the decreasing temperature [Fig. 7(a)]. All of this means that the WL correction for the patterned structure is not described by Eq. (4) and the determination of the phase breaking time by the standard way is impossible.[22]

The strong sensitivity of the fitting parameters to the fitting interval width indicates that the role of dielectric antidots in 2D gas is not reduced to the presence of the prefactor $\exp(-\tau_E/\tau_\phi)$ with τ_E the Ehrenfest time, which suppresses the weak localization in the 2D gas with hard disks as scatterers.[6,23,24]

Specific features of the weak localization in the patterned sample can be understood by considering the quasiclassic interpretation of this phenomenon. Within quasiclassic approximation, the WL correction is expressed through the classical probability density $\mathcal{W}$ that an electron returns to the area of the order $\lambda_F l$ (where $\lambda_F=2\pi/k_F$ with k_F as the Fermi wave vector) around the starting point,[25–28]

$$\delta\sigma = -\sigma_0 \frac{\lambda_F l}{\pi}\mathcal{W}, \tag{5}$$

where $\sigma_0=\pi k_F l G_0$ is the Drude conductivity. Taking into account the inelastic processes and the presence of external magnetic field, Eq. (5) can be written as follows:[29]

$$\delta\sigma(b) = -2\pi l^2 G_0 \int_{-\infty}^{\infty} dS W(S) \exp\left[-\frac{\bar{L}(S)}{l_\phi}\right] \cos\left(\frac{bS}{l^2}\right). \tag{6}$$

Here, l_ϕ is the phase breaking length connected with τ_ϕ through the Fermi velocity, $l_\phi=v_F\tau_\phi$, and $W(S)$ and $\bar{L}(S)$ are the algebraic area distribution function of closed paths and the area dependence of the average length of closed paths, respectively (for more detail, see Sec. II of Ref. 29). This equation shows that the shape of the magnetoconductivity curve is determined by the statistics of the closed paths, namely, by the area distribution function $W(S)$ and by function $\bar{L}(S)$. It is clear that the existence of dielectric dots in 2D gas should change the statistics of closed paths resulting in the change in the shape of the magnetoconductivity curve. In Ref. 30, there it is shown how the analysis of the Fourier transform of the negative magnetoresistance provides the information on the function $W(S)$. The short of the matter is clear from Eq. (6). It is seen that the Fourier transform of $\delta\sigma(B)$

$$\Phi(S) = \frac{1}{\Phi_0}\int_{-\infty}^{\infty} dB\, \delta\sigma(B) \cos\left(\frac{2\pi BS}{\Phi_0}\right)$$

is equal to

$$\Phi(S) = -2\pi l^2 G_0 W(S) \exp\left(-\frac{\bar{L}(S)}{l_\phi}\right), \tag{7}$$

where $\Phi_0=\pi\hbar/e$ is the elementary flux quantum. It is apparent that $\Phi(S)\to -2\pi l^2 G_0 W(S)$ at $T\to 0$ because l_ϕ tends to infinity with decreasing temperature. Thus, taking the Fourier transform from the magnetoconductivity curves measured at different temperatures and extrapolating $\Phi(S)$ to $T=0$, we experimentally obtain the area distribution function $W(S)$.

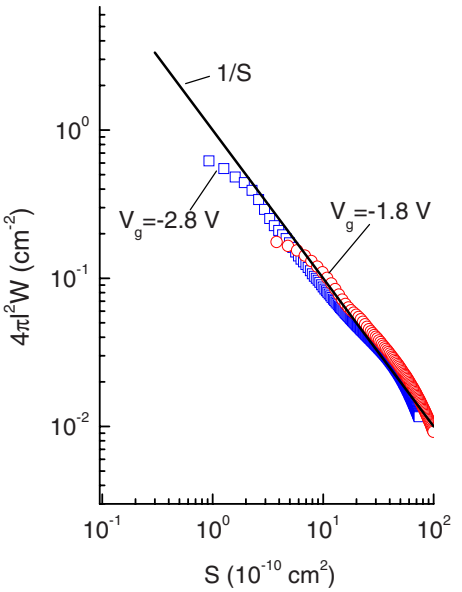

FIG. 8. (Color online) The area distribution function $W(S)$ obtained experimentally for the unpatterned samples for two gate voltages (symbols). Line is the diffusion limit: $4\pi l^2 W=1/S$.

The results of such data treatment for the unpatterned and patterned samples are shown in Figs. 8 and 9(a), respectively (note the scales in these figures are identical). One can see that not only the W-vs-S dependences are drastically different for the patterned and unpatterned samples but their responses to the change in the gate voltage are different as well. The area distribution function for the unpatterned sample is very close to that predicted theoretically for 2D homogeneous systems in the diffusion regime $4\pi l^2 W=S^{-1}$, $S>l^2$ (see Refs. 29 and 30); it is practically insensitive to the

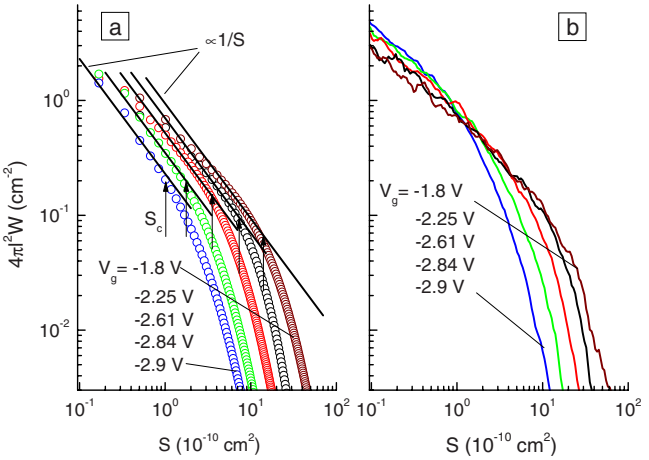

FIG. 9. (Color online) (a) The function $4\pi l^2 W(S)$ obtained experimentally for the patterned sample for different gate voltages. Arrows indicate where the plots deviate from $1/S$ dependence. (b) The function $4\pi l^2 W(S)$ obtained from the simulation procedure. The parameters correspond to the gate voltages in panel (a).

gate voltage (Fig. 8). As for the patterned sample, it is seen from Fig. 9(a) that the curves follow near the $1/S$ dependence only at low S values $S<S_c$. At higher areas $S>S_c$, W decreases when S increases much steeper than S^{-1}; the lower gate voltage is the lower areas S_c at which this deviation occurs. It should be noted that such an approach allows us to obtain experimentally the area distribution function of the trajectories which length is less than approximately $2l'_\phi$, where l'_ϕ is the phase relaxation length at the lowest temperature of the experiment because the contribution of longer trajectories to the magnetoconductivity is very small.

Before interpreting such a behavior of $W(S)$ for the patterned sample, let us clarify the meaning of this quantity for this case. Because our system is inhomogeneous due to dielectric inclusions under the holes in the cap layer, Eq. (6) should be rederived. This is because the function $W(S)$ is not universal now, it depends on the position of the start point. If one neglects as above the aperiodicity of the antidots array, we obtain the following expression connecting the correction to the conductivity of the antidots array and the local correction $\delta\sigma_l$:

$$\delta\sigma(b) = \frac{\int \frac{dy}{[w(y)]^2} \int dx\, \delta\sigma_l(x,y,b)}{\left[\int \frac{dy}{w(y)}\right]^2}. \tag{8}$$

Here, the integration runs over the intervals given by the border of conducting area, $w(y)$ is the y dependence of width of conducting area, and the quantity $\sigma_l(x,y,b)$ is given by the expression analogous to Eq. (6),

$$\delta\sigma_l(x,y,b) = -2\pi l^2 G_0 \int_{-\infty}^{\infty} dS \left\{ \mathfrak{W}(x,y,S) \times \exp\left[-\frac{\bar{L}(x,y,S)}{l_\phi}\right] \cos\left(\frac{bS}{l^2}\right) \right\}, \tag{9}$$

in which $\mathfrak{W}(x,y,S)$ is determined in such a way that $\mathfrak{W}(x,y,S)dS$ gives the density probability of return to the starting point with the coordinates (x,y) with the enclosed algebraic area in the interval $(S,S+dS)$.

Thus, the above described procedure, which for the homogeneous 2D gas allows us to obtain the area distribution function of closed paths, being applied to the data obtained for the patterned sample gives the *effective* area distribution function,

$$W(S) = \frac{\int \frac{dy}{[w(y)]^2} \int \mathfrak{W}(x,y,S)dx}{\left[\int \frac{dy}{w(y)}\right]^2}. \tag{10}$$

Now we are in position to discuss the behavior of $W(S)$ for the patterned sample [Fig. 9(a)]. In order to understand the main features we have performed the computer simulation of a particle motion over 2D plane with scatterers. The details can be found in Refs. 29, 31, and 32; below is an outline with the important features only. The 2D plane is represented as a lattice with scatterers of two types placed in a part of lattice site. The scatterers of the first type with isotropic differential cross section determine the local mobility. The scatterers of the second type are hard disks with specular reflection from the boundaries.[33] Particle motion is forbidden within the disks. They correspond to the areas of 2D gas under the holes. A particle is launched from some point with x,y as coordinates then it moves with a constant velocity along straight lines, which happen to be terminated by collisions with the scatterers. After a collision it changes its direction in motion. If the particle passes near the starting point at a distance less than some prescribed value $a/2 \ll l$, the path is considered being closed.

Its length and enclosed algebraic area are calculated and kept in the computer memory. The particle walks over the plane until the path traversed is longer than $2l'_\phi$, where l'_ϕ is the phase relaxation length obtained at the lowest temperature on the unpatterned sample for the same V_g value. As mentioned above, the statistics of such closed paths can be reliably obtained from the weak localization experiments. When the path becomes longer than this value, another particle is launched and all is repeated. After a large number of launches from the starting point with given x,y coordinates, $\mathfrak{W}(x,y,S)$ is calculated as

$$\mathfrak{W}(x,y,S) = \frac{n_S}{Nla\Delta S}, \tag{11}$$

where N is the number of starts from this point, n_S is the number of returns along the trajectory with the enclosed area in the interval $(S,S+\Delta S)$. Launching the particle from different starting points, we are able to calculate numerically the function $W(S)$ using Eq. (10) in the discrete form.

Shown in Fig. 9(b) are the results of simulation procedure carried out with the parameters corresponding to the gate voltages from Fig. 9(a). It is clearly seen that the results of computer simulation are in qualitative agreement with those of the real experiment; both simulated and experimental curves demonstrate a steep fall at large S that shifts to lower areas with decreasing gate voltage. Some discrepancy between the experimental and the simulation results evident at low S is due to the crudity of our model. We use the model of local conductivity. This model works well when the mean free path is much smaller than all the characteristic scales of the system. If one compares the mean free path with the channel width, we can see that they are close to each other. Because the main contribution to W at small S comes from the narrow where the collisions with the antidots occur rather often, this model fails. The trajectories responsible for W behavior at large S are significantly longer. They extend beyond the channels into the lakes where the collisions with the antidots occur rarely as compared with the collisions with scatterers. Therefore, the model of the local conductivity works better and describes the main features of $W(S)$ evident at large S. The other point is that the experimental w_0 value is used in the simulation. As seen from Fig. 4(b) the error in w_0 is sufficiently large, especially at low electron density when the channels are narrow. A change in w_0 within the experimental error shifts the simulated curves vertically so

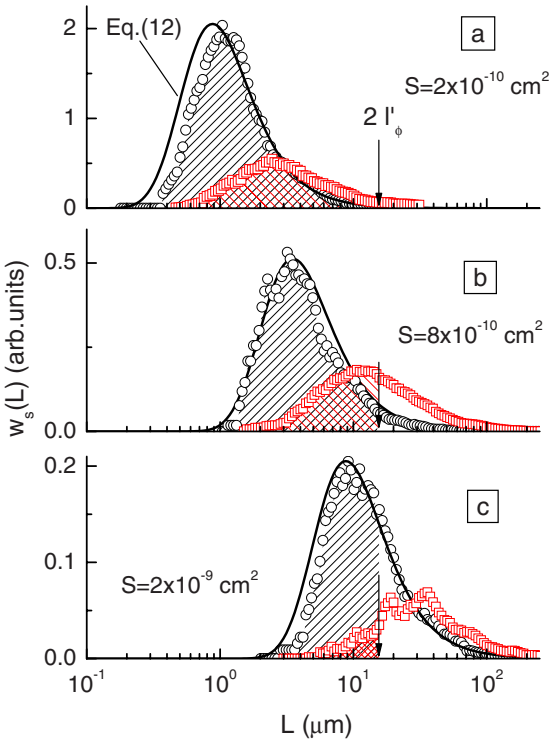

FIG. 10. (Color online) The length distribution functions of closed paths with different area enclosed obtained from the simulation procedure with parameters corresponding to the unpatterned (circles) and patterned (squares) samples for $V_g=-2.84$ V. Lines are calculated from Eq. (12) with corresponding S values and $l=0.06$ μm. Hatched areas are the W value for paths with $L\leq 2l'_\phi$.

that the accordance with the experiment is somewhat improved.

Analysis of the simulation results gives an insight into why the experimental W vs S dependence is steeper for the patterned sample. This can be done if one considers how the paths with the given area enclosed are distributed over the length. This distribution is characterized by the function $w_S(L)$ determined in such a way that $w_S(L)dS$ gives the density probability of return along a trajectory with the length L and area in the interval $(S,S+dS)$. In Fig. 10 we show the functions $w_S(L)$ obtained from the simulation procedure for the patterned[34] and unpatterned samples (all the paths including those for which $L>2l'_\phi$ are taken into account here). Qualitatively, the functions are similar. They have a peak which position characterizes the typical length of closed paths. In both cases, the larger area enclosed the longer trajectories. The w_S vs L plot for the unpatterned sample is well described by the expression

$$w_S(L)=\frac{1}{(2lL)^2}\cosh^{-2}\left(\frac{\pi S}{lL}\right) \tag{12}$$

obtained analytically within the diffusion approximation for the homogeneous 2D system[29] that justifies the validity of simulation procedure. An important point is that the closed paths in the patterned sample are significantly longer than the paths in the unpatterned sample with the same area enclosed. If, in correspondence with the experimental situation, one

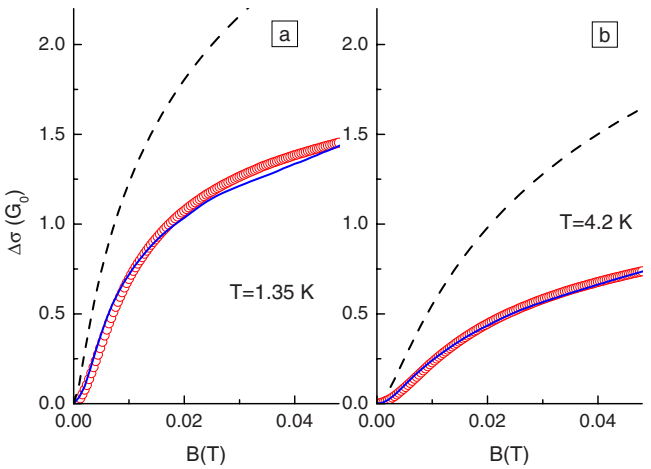

FIG. 11. (Color online) The low-field magnetoconductance for the patterned sample for (a) $T=1.35$ and (b) 4.2 K, $V_g=-2.25$ V. Symbols are the measured dependences. Solid and dashed lines are the simulation results and Eq. (4), respectively, obtained with (a) $\tau_\phi=1.9\times10^{-11}$ s and (b) $\tau_\phi=6.8\times10^{-12}$ s.

restricts the consideration by short trajectories $L\lesssim 2l'_\phi$, we obtain

$$W(S)=\int_0^{2l'_\phi} w_S(L)\frac{dL}{l} \tag{13}$$

approximately the same for the both samples when S is relatively small [Figs. 10(a)] and much less in the patterned sample when S is sufficiently large [Fig. 10(c)]. Thus, the different length distribution of closed paths is the reason for the different behavior of the area distribution function obtained experimentally for the patterned and unpatterned samples.

Let us return to the magnetoconductivity caused by suppression of the interference quantum correction. The simulation procedure allows us to find $\delta\sigma(b)$ for the model system with the use of Eq. (8) in the discrete form and $\delta\sigma_l(x,y,b)$ calculated as

$$\delta\sigma_l(x_i,y_i,b)=\frac{2\pi lG_0}{dN_i}\sum_k \cos\left(\frac{bS_i^k}{l^2}\right)\exp\left(-\frac{l_i^k}{l_\phi}\right), \tag{14}$$

where summation runs over all closed trajectories among a total number of trajectories N_i starting from the point with x_i and y_i as coordinates and S_i^k and l_i^k stand for algebraic area and length of the kth trajectory, respectively.

In Fig. 11 we compare the simulation and experimental results. Symbols are the experimental plot obtained for the patterned sample at $V_g=-2.25$ V. Solid lines are $\Delta\sigma=\delta\sigma(B)-\delta\sigma(0)$ for the model system. The values of $\tau_\phi=1.9\times10^{-11}$ s for $T=1.35$ K and $\tau_\phi=6.8\times10^{-12}$ s for $T=4.2$ K correspond to the best accordance with the experimental data. It is significant that they are close to that obtained for the unpatterned sample [see Fig. 7(a)]. If one calculates $\Delta\sigma(B)$ from Eq. (4) with the same parameters and $\alpha=1$, we obtain drastic disagreement with the experimental magnetoconductivity.

Thus, the simulation approach allows us to understand

qualitatively the main features of the low-field magnetoconductivity in the patterned samples, which are determined by the peculiarities of statistics of closed paths. It would serve no purpose to make more detailed comparison between the experimental and simulation results because our model is rather crude. We supposed that the areas forbidden for classical motion had the form of disks. As seen from Fig. 1(b), this is not exactly the case. Moreover, the mean free path and Fermi velocity are not constant over the conducting area as it has been assumed.

In summary, we have studied the weak localization in the 2D electron gas with potential electrostatic relief forming the insulating antidots array. It has been shown that the use of the standard procedure for obtaining the phase relaxation time from the shape of the magnetoconductivity curve is inadequate when it is applied to the antidots array structure in the diffusion regime. To understand the main features of the weak localization in these systems, an alternative approach based on the analysis of the statistics of closed paths has been used. We have shown that the main peculiarities of the WL phenomenon in the patterned structure are due to the specific statistics of closed paths. The paths of actual areas in system with antidots are characterized by significantly larger lengths as compared with the usual 2D systems.

We are grateful to I. V. Gornyi for very useful discussions and S. V. Dubonos for sample fabrication. This work was supported in part by the RFBR (Grants No. 06-02-16292, No. 07-02-00528, and No. 08-02-00662) and the CRDF (Grant No. Y3-P-05-16).

[1] K. Ensslin and P. M. Petroff, Phys. Rev. B **41**, 12307 (1990).
[2] D. Weiss, M. L. Roukes, A. Menschig, P. Grambow, K. von Klitzing, and G. Weimann, Phys. Rev. Lett. **66**, 2790 (1991).
[3] A. M. Chang, H. U. Baranger, L. N. Pfeiffer, and K. W. West, Phys. Rev. Lett. **73**, 2111 (1994).
[4] M. V. Budantsev, Z. D. Kvon, A. G. Pogosov, G. M. Gusev, J. C. Portal, D. K. Maude, N. T. Moshegov, and A. I. Toropov, Physica B **256-258**, 595 (1998).
[5] Oleg Yevtushenko, Gerd Lutjering, Dieter Weiss, and Klaus Richter, Phys. Rev. Lett. **84**, 542 (2000).
[6] J. A. Folk, C. M. Marcus, and J. S. Harris, Phys. Rev. Lett. **87**, 206802 (2001).
[7] A. Pouydebasque, A. G. Pogosov, M. V. Budantsev, A. E. Plotnikov, A. I. Toropov, D. K. Maude, and J. C. Portal, Phys. Rev. B **64**, 245306 (2001).
[8] Z. D. Kvon, Pis'ma Zh. Eksp. Teor. Fiz. **76**, 619 (2002) [JETP Lett. **76**, 537 (2002)].
[9] August Dorn, Thomas Ihn, Klaus Ensslin, Werner Wegscheider, and Max Bichler, Phys. Rev. B **70**, 205306 (2004).
[10] M. Ferrier, L. Angers, A. C. H. Rowe, S. Gueron, H. Bouchiat, C. Texier, G. Montambaux, and D. Mailly, Phys. Rev. Lett. **93**, 246804 (2004).
[11] B. Hackens, S. Faniel, C. Gustin, X. Wallart, S. Bollaert, A. Cappy, and V. Bayot, Phys. Rev. Lett. **94**, 146802 (2005).
[12] I. L. Aleiner and A. I. Larkin, Phys. Rev. B **54**, 14423 (1996).
[13] D. G. Polyakov, F. Evers, A. D. Mirlin, and P. Wölfle, Phys. Rev. B **64**, 205306 (2001).
[14] P. W. Brouwer, J. N. H. J. Cremers, and B. I. Halperin, Phys. Rev. B **65**, 081302(R) (2002).
[15] D. S. Golubev and A. D. Zaikin, Phys. Rev. B **74**, 245329 (2006).
[16] Iva Brezinova, Christoph Stampfer, Ludger Wirtz, Stefan Rotter, and Joachim Burgdörfer, Phys. Rev. B **77**, 165321 (2008).
[17] G. M. Minkov, A. V. Germanenko, O. E. Rut, A. A. Sherstobitov, V. A. Larionova, A. K. Bakarov, and B. N. Zvonkov, Phys. Rev. B **74**, 045314 (2006).
[18] Another way of describing the positive magnetoresistance is considering the interplay between short- and long-range disorders in the magnetic field (see Ref. 14).
[19] S. Hikami, A. Larkin, and Y. Nagaoka, Prog. Theor. Phys. **63**, 707 (1980).
[20] H.-P. Wittmann and A. Schmid, J. Low Temp. Phys. **69**, 131 (1987).
[21] A. V. Germanenko, V. A. Larionova, I. V. Gornyi, and G. M. Minkov, Int. J. Nanosci. **6**, 261 (2007).
[22] In this connection the low-T saturation of τ_ϕ reported in some paper for granular metal films [see, e.g., X. X. Zhang, Chuncheng Wan, H. Liu, Z. Q. Li, P. Sheng, and J. J. Lin, Phys. Rev. Lett. **86**, 5562 (2001)] is questionable.
[23] I. L. Aleiner and A. I. Larkin, Phys. Rev. B **54**, 14423 (1996); Chaos, Solitons Fractals **8**, 1179 (1997).
[24] Robert S. Whitney, Philippe Jacquod, and Cyril Petitjean, Phys. Rev. B **77**, 045315 (2008).
[25] L. P. Gorkov, A. I. Larkin, and D. E. Khmelnitskii, Pis'ma Zh. Eksp. Teor. Fiz. **30**, 248 (1979) [JETP Lett. **30**, 228 (1979)].
[26] S. Chakravarty and A. Schmid, Phys. Rep. **140**, 193 (1986).
[27] M. I. Dyakonov, Solid State Commun. **92**, 711 (1994).
[28] A. P. Dmitriev, V. Yu. Kachorovskii, and I. V. Gornyi, Phys. Rev. B **56**, 9910 (1997).
[29] G. M. Minkov, A. V. Germanenko, V. A. Larionova, S. A. Negashev, and I. V. Gornyi, Phys. Rev. B **61**, 13164 (2000).
[30] G. M. Minkov, S. A. Negashev, O. E. Rut, A. V. Germanenko, O. I. Khrykin, V. I. Shashkin, and V. M. Daniltsev, Phys. Rev. B **61**, 13172 (2000).
[31] A. V. Germanenko, G. M. Minkov, and O. E. Rut, Phys. Rev. B **64**, 165404 (2001).
[32] A. V. Germanenko, G. M. Minkov, A. A. Sherstobitov, and O. E. Rut, Phys. Rev. B **73**, 233301 (2006).
[33] The simulation results presented in the paper are practically the same for the diffusive reflection from the hard disks.
[34] For the patterned sample, the effective length distribution function defined by analogy with Eq. (10) is presented.